Supporting Information

Computational Design of a Time-Dependent Histone Deacetylase 2 Selective Inhibitor

Jingwei Zhou[1], *Min Li*[1], *Nanhao Chen*[1], *Shenglong Wang*[2], *Hai-Bin Luo*[1], *Yingkai Zhang*[1, 2*], *and Ruibo Wu*[†*]

[1] School of Pharmaceutical Sciences, Sun Yat-sen University, Guangzhou 510006, P.R. China

[2] Department of Chemistry, New York University, New York, New York 10003, United States

[3] NYU-ECNU Center for Computational Chemistry at NYU Shanghai, Shanghai 200062, P.R. China

Benchmark test on the non-enzyme and corresponding enzyme models

The DFT calculations on the selected simplified non-enzyme models were prepared to probe the reactivity of the intramolecular nucleophilic attack reaction controlled by R_1/ R_2. As shown in Figure S3, both the stepwise and concerted reaction mechanisms were considered. The reactant and product structures as well as transition states were optimized at the level of M06-2X/6-311+G** in the gas phase. Based on these stationary structures, the relative reaction free energy profiles were further obtained from frequency analysis at the same theoretical level with PCM solvent continuum models (CCl4, CHCl3 and water were considered). And all these calculation were carried out in Gaussian 09 package.

As shown in Figure S4(a), It fails to obtain the transition state under the stepwise mechanism(Scheme I in Figure S3). The relative free energy profiles of the concerted reaction mechanisms (Scheme II in Figure S3) are shown in Figure S4(b-c). It indicates that the intramolecular nucleophilic attack reactivity could be modulated by the R_1 and R_2 groups. And further QM/MM calculations indicate that the reactivity would be highly increased under enzyme catalysis (the computational details are presented in the "Experimental and Computational details" section and Figure S5-S6, and the results are summarized in Figure S7). All the reaction barriers of these modes are summarized in Table S1.

Structure Determination of the *β*-aminomethyl and *β*-hydroxymethyl chalcone

(Z)-4-Amino-1,3-diphenylbut-2-en-1-one (β-aminomethyl chalcone). A brown and green solid, ~21.4% yield. 90% pure. 1H NMR (400 MHz, CDCl3): δ1.29(s, 2H, NH2), 4.61(s, 2H, CH2), 6.86(s, 2H, ArH), 7.17-7.42(m, 7H, ArH), 8.51(s, 2H, ArH). 13C NMR (100 MHz, CDCl3) δ 190.7, 155.9, 136.4, 135.6, 134.1, 128.4, 128.1, 127.5, 126.1, 124.8, 108.9, 59.2 ESI-MS(m/z)=237.02[M]+

(Z)-4-Hydroxy-1,3-diphenylbut-2-en-1-one (β-hydroxymethyl chalcone). A pale yellow oil, 10.11% yield. 96% pure. 1H NMR (400 MHz, CDCl3): δ5.50(s, 2H, CH2), 7.16-7.57(m, 9H, ArH), 8.00-8.01(d, J = 4Hz, 2H, ArH). 13C NMR (100 MHz, CDCl3) δ 188.9, 150.5, 140.7, 136.5, 133.6, 128.4, 127.5, 127.1, 126.3, 124.7, 104.5, 51.2 ESI-MS(m/z)=237.94[M]+

Experimental and Computational details

Fluorogenic Assay of HDAC Inhibition Activities.

In the first step, an acetylated lysine substrate was incubated with HDAC1-3 for 30 minutes at 37℃. Deacetylation sensitized the substrate with HDAC developer in the second step released a fluorescent product. The fluorophore was easily analyzed using a fluorescence plate reader with excitation wavelength of 347 nm and emission wavelength of 465 nm. A hydroxamic acid HDAC inhibitor (TSA)[1] which was applied to terminate the incubation process was added to HDAC developer before the second step. The assay buffer (25 mM Tris-HCl, pH 8.0, 137 mM NaCl, 2.7 mM KCl and 1 mM MgCl2), TSA (0.21 mM), acetylated lysine substrate (3.4 mM) and HDAC developer were purchased from Cayman (U.S.A). The human recombinant HDAC1, HDAC2 and HDAC3 were purchased from Epigentek (U.S.A). And the benzamide-like inhibitor MS-275 compound was purchased from Wuhan NCE Biomedical Co.,Ltd (China).

All assays were performed according to the protocol of HDAC1 inhibitor screening assay kit. First, 140 μL assay buffer was added into a well on a 96-well plate. HDAC enzymes were diluted to the desired concentrations with assay buffer and then, 10 μL diluted enzyme was dispensed into the well. Second, *β*-substituted chalcones and MS-275 were dissolved in assay buffer primarily, and a series of five-fold dilutions of each compound were prepared with assay buffer. 10 μL of each dilution was also added into the correspondent well to mix with enzyme at room temperature. Third, 10 μL acetylated lysine substrate was added to correspondent well to initiate deacetylation reaction after the mixture above had been mixed at room temperature

for 1 hours. The deacetylation reaction was kept up for 30 minutes on a shaker at 37℃. Finally, 40 μL HDAC developer which included TSA used to terminate the deacetylation process was assigned to the well to combine with the deacetylated lysine for 15 minutes on a shaker at room temperature. The fluorescence intensity of the combination product was measured on a microplate reader (Flex Station 3, Moleculardevices) in 30 minutes using an excitation wavelength of 340-360 nm and an emission wavelength of 440-465 nm. In addition, the fluorescence intensity of the 100% initial activity without enzyme (F100) and background activity without inhibitors (F0) were also taken into account to equilibrate the assay result. The fluorescence intensity data were analyzed by Origin software. So in the presence of inhibitors and HDAC enzymes, the fluorescence intensity (F) was laid between F0 and F100. And the accurate relative HDAC activity was calculated based on the following equation: %activity = (F-F0)/(F100-F0). The TSA inhibitor was also employed as the positive control to demonstrate the reliability of the method above. Each assay was repeated three times and the mean values were used for S curve fitting to obtain the IC50 values.

To further test the time-dependent inhibition of chemicals, 10 μL of diluted β-hydroxymethyl chalcone was mixed with or without enzyme at room temperature for 4 hours, 8 hours, 12 hours, 16 hours, 20 hours and 24 hours, respectively. Then 10 μL acetylated lysine substrate was added to initiate deacetylation reaction. Fluorescence intensity was recorded at each time point to calculate time-dependent inhibition.

Preparation of the HDAC1/2/3-Ligand Complexes.

The HDAC2-benzamide complex was built based on the crystal structure (pdb code: 3MAX)[2]. And then the two HDAC2-*β*-substituted chalcones complexes were obtained from manual docking based on the benzamide skeleton. First, the protonation states of charged residues were determined in consistent with our previous study[3-5], His183 was determined as singly protonated on ε site, while His145 and His146 was determined as singly protonated on δ site. Then, several Na+ ions were added around the protein surface to neutralize the total charges for each model, and then solvated into a cubic water box with an 8 Å distance between the solvent box wall and the nearest solute atoms. The TIP3P model[6] and Amber99SB force field[7-9] were employed for the water and protein respectively, while the force field parameters of each ligand was generated from AMBER GAFF force field[10]. The partial atomic charges of these ligands were obtained from the restrained electrostatic potential (RESP) charge based on HF/6-31G* calculation with Gaussian09 package[11].

All of the prepared systems were minimized and equilibrated step by step. After several steps of minimization, the heating MD simulation was performed from 0 K to 300 K gradually under the NVT ensemble for 50 ps. Then 100 ps MD simulations were performed under the NPT ensemble to relax the system density to be about 1.0 g/cm3, with the target temperature of 300 K and the target pressure of 1.0 atm. And then further equilibrated for ~50 ns by employing GPU-accelerated AMBER12 package[12]. The MD trajectories were very stable after ~0.5 ns and the resulted snapshots were employed for subsequent QM/MM calculation. During the MD simulations, the SHAKE algorithm[13] was applied to constrain all hydrogen-containing

bonds with a tolerance of 10^{-5}. The Berendsen thermostat[14] method was used to control the system temperature and a cutoff of 12 Å was set for both van der Waals and electrostatic interactions. The preparation of the HDAC1/3-Ligand complexes was followed by the same steps based on the HDAC1/3 crystal structures (pdb code: 4BKX & 4A69, respectively)[15, 16].

Born-Oppenheimer ab initio QM/MM MD simulations.

Each cubic system from above molecular dynamics simulations was cut into a sphere by removing the solvent water molecules which were beyond 30 Å of the zinc ion in the active site. Then, the resulted systems were partitioned into QM and MM subsystems. The His145, His146, Asp181, His183, Asp269, ligands and zinc ion were chosen as the QM subsystem (showed in Figure S5) which was treated by M06-2X[17, 18] with Stuttgart ECP/basis set (SDD) for the zinc atom and 6-31G* basis set for all other QM atoms. In comparison with B3LYP, M06-2X method was more adaptive to characterize a cyclization reaction in previous study[17-21]. Nevertheless, primary benchmark test on the B3LYP and M06-2X methods have been performed (see Figure S4(d) and Figure S7(e-f)). The QM/MM boundaries were described by the pseudobond approach[22-25] with the improved pseudobond parameters. All the left atoms were described by the same molecular mechanical force field used in previous classical MD simulations. For all QM/MM calculations, the spherical boundary condition was applied and the atoms more than 20 Å away from the zinc atom were fixed. The 18 Å and 12 Å cutoffs were employed for electrostatic and van der Waals interactions, respectively. There was no cutoff for electrostatic interactions between QM and MM regions. The prepared QM/MM systems were first minimized, and then

25 ps QM/MM MD simulations were performed with the time step of 1 fs and the Beeman algorithm[26] to integrate the Newton equations of motion, as well as the Berendsen thermostat method[14] to control the system temperature at 300 K. The configurations of last 20 ps were collected for data analysis. All our ab initio QM/MM calculations were performed in modified QChem-Tinker programs[27, 28]. As shown in Figure S10 (a-b), the representative zinc chelation modes and hydrogen bond network around the benzamide in HDAC2 from our QM/MM MD simulations are consistent with the XRD structure, thus our simulation protocols are reasonable.

Furthermore, to study the intramolecular nucleophilic attack reaction, the resulting structures from QM/MM MD simulations of the two HDAC2-chalcones were first minimized to map out the minimum energy paths with reaction coordinate driving method[24]. The determination of reaction coordinate was presented in Figure S6 and S7. For each determined structure along the minimum energy paths, the MM subsystem was equilibrated with 500 ps molecular mechanical MD simulation with the QM subsystem fixed. And then, each resulting snapshot was employed as the starting structure to carry out 20 ps ab initio QM/MM MD simulations with umbrella sampling[29, 30]. The configurations of the last 15 ps at each window were collected for data analysis. The probability distributions along the reaction coordinate were determined for each window and pieced together with the WHAM[31, 32] to yield the reaction free energy profile. The setup for QM/MM MD simulations of HDAC1/3-chalcone complexes was similar to that of HDAC2-chalcone model.

References

1. Vigushin, D. M., Ali, S., Pace, P. E., Mirsaidi, N., Ito, K., Adcock, I., and Coombes, R. C. (2001) Trichostatin A is a histone deacetylase inhibitor with potent antitumor activity against breast cancer in vivo, *Clin. Cancer. Res. 7*, 971-976.
2. Bressi, J. C., Jennings, A. J., Skene, R., Wu, Y., Melkus, R., De Jong, R., O'Connell, S., Grimshaw, C., Navre, M., and Gangloff, A. R. (2010) Exploration of the HDAC2 foot pocket: Synthesis and SAR of substituted N-(2-aminophenyl)benzamides, *Bioorg. Med. Chem. Lett. 20*, 3142-3145.
3. Wu, R., Hu, P., Wang, S., Cao, Z., and Zhang, Y. (2010) Flexibility of Catalytic Zinc Coordination in Thermolysin and HDAC8: A Born-Oppenheimer ab initio QM/MM Molecular Dynamics Study, *J. Chem. Theory Comput. 6*, 337-343.
4. Wu, R., Lu, Z., Cao, Z., and Zhang, Y. (2011) Zinc chelation with hydroxamate in histone deacetylases modulated by water access to the linker binding channel, *J. Am. Chem. Soc. 133*, 6110-6113.
5. Wu, R., Wang, S., Zhou, N., Cao, Z., and Zhang, Y. (2010) A proton-shuttle reaction mechanism for histone deacetylase 8 and the catalytic role of metal ions, *J. Am. Chem. Soc. 132*, 9471–9479.
6. Jorgensen, W. L., Chandrasekhar, J., Madura, J. D., Impey, R. W., and Klein, M. L. (1983) Comparison of Simple Potential Functions for Simulating Liquid Water, *J. Chem. Phys. 79*, 926-935.
7. Cornell, W. D., Cieplak, P., Bayly, C. I., Gould, I. R., Merz, K. M., Ferguson, D. M., Spellmeyer, D. C., Fox, T., Caldwell, J. W., and Kollman, P. A. (1995) A Second Generation Force Field for the Simulation of Proteins, Nucleic Acids, and Organic Molecules, *J. Am. Chem. Soc. 117*, 5179-5197.
8. Wang, J. M., Cieplak, P., and Kollman, P. A. (2000) Geometrical and electronic structure variability of the sugar-phosphate backbone in nucleic acids, *J. Comput. Chem. 21*, 1049-1074.
9. Hornak, V., Abel, R., Okur, A., Strockbine, B., Roitberg, A., and Simmerling, C. (2006) Comparison of multiple Amber force fields and development of improved protein backbone parameters, *Proteins: Struct., Funct., Bioinf. 65*, 712-725.
10. Wang, J. M., Wolf, R. M., Caldwell, J. W., Kollman, P. A., and Case, D. A. (2004) Development and testing of a general amber force field, *J. Comput. Chem. 25*, 1157-1174.
11. Frisch, M. J., Trucks, G. W., Schlegel, H. B., Scuseria, G. E., Robb, M. A., Cheeseman, J. R., Scalmani, G., Barone, V., Mennucci, B., Petersson, G. A., Nakatsuji, H., Caricato, M., Li, X., Hratchian, H. P., Izmaylov, A. F., Bloino, J., Zheng, G., Sonnenberg, J. L., Hada, M., Ehara, M., Toyota, K., Fukuda, R., Hasegawa, J., Ishida, M., Nakajima, T., Honda, Y., Kitao, O., Nakai, H., Vreven, T., Montgomery Jr, J. A., Peralta, J. E., Ogliaro, F., Bearpark, M., Heyd, J. J., Brothers, E., Kudin, K. N., Staroverov, V. N., Kobayashi, R., Normand, J., Raghavachari, K., Rendell, A., Burant, J. C., Iyengar, S. S., Tomasi, J., Cossi, M., Rega, N., Millam, J. M., Klene, M., Knox, J. E., Cross, J. B., Bakken, V., Adamo, C., Jaramillo, J., Gomperts, R., Stratmann, R. E.,

Yazyev, O., Austin, A. J., Cammi, R., Pomelli, C., Ochterski, J. W., Martin, R. L., Morokuma, K., Zakrzewski, V. G., Voth, G. A., Salvador, P., Dannenberg, J. J., Dapprich, S., Daniels, A. D., Farkas, Ö., Foresman, J. B., Ortiz, J. V., Cioslowski, J., and Fox, D. J. (2009) in *Gaussian, Inc.,Wallingford CT.*

12. Case, D. A., Darden, T. A., Cheatham, I., T.E., Simmerling, C. L., J. Wang, Duke, R. E., Luo, R., Walker, R. C., Zhang, W., Merz, K. M., Roberts, B., Hayik, S., Roitberg, A., Seabra, G., Swails, J., Götz, A. W., Kolossváry, I., Wong, K. F., Paesani, F., Vanicek, J., Wolf, R. M., Liu, J., Wu, X., Brozell, S. R., Steinbrecher, T., Gohlke, H., Cai, Q., Ye, X., Wang, J., Hsieh, M.-J., Cui, G., Roe, D. R., Mathews, D. H., Seetin, M. G., Salomon-Ferrer, R., Sagui, C., Babin, V., Luchko, T., Gusarov, S., Kovalenko, A., and Kollman, P. A. (2012) *AMBER 12, University of California, San Francisco.*
13. Ryckaert, J. P., Ciccotti, G., and Berendsen, H. J. C. (1977) Numerical integration of the cartesian equations of motion of a system with constraints: molecular dynamics of n-alkanes, *J. Comput. Phys. 23*, 327-341.
14. Berendsen, H. J. C., Postma, J. P. M., Van Gunsteren, W. F., DiNola, A., and Haak, J. R. (1984) Molecular dynamics with coupling to an external bath, *J. Chem. Phys. 81*, 3684-3690.
15. Millard, C. J., Watson, P. J., Celardo, I., Gordiyenko, Y., Cowley, S. M., Robinson, C. V., Fairall, L., and Schwabe, J. W. (2013) Class I HDACs share a common mechanism of regulation by inositol phosphates, *Mol. Cell 51*, 57-67.
16. Watson, P. J., Fairall, L., Santos, G. M., and Schwabe, J. W. (2012) Structure of HDAC3 bound to co-repressor and inositol tetraphosphate, *Nature 481*, 335-340.
17. Zhao, Y., and Truhlar, D. G. (2008) The M06 suite of density functionals for main group thermochemistry,thermochemical kinetics, noncovalent interactions, excited states, and transition elements: two new functionals and systematic testing of four M06-class functionals and 12 other functionals, *Theor. Chem. Acc. 120*, 215-241.
18. Zhao, Y., and Truhlar, D. G. (2008) Exploring the Limit of Accuracy of the Global Hybrid Meta Density Functional for Main-Group Thermochemistry, Kinetics, and Noncovalent Interactions, *J.Chem.Theory.Comput. 4*, 1849-1868.
19. Breugst, M., Eschenmoser, A., and Houk, K. N. (2013) Theoretical exploration of the mechanism of riboflavin formation from 6,7-dimethyl-8-ribityllumazine: nucleophilic catalysis, hydride transfer, hydrogen atom transfer, or nucleophilic addition, *J. Am. Chem. Soc. 135*, 6658.
20. Lopez, S. A., Munk, M. E., and Houk, K. N. (2013) Mechanisms and transition states of 1,3-dipolar cycloadditions of phenyl azide with enamines: a computational analysis, *J. Org. Chem. 78*, 1576.
21. Chen, N., Zhou, J., Li, J., Xu, J., and Wu, R. (2014) Concerted Cyclization of Lanosterol C-Ring and D-Ring Under Human Oxidosqualene Cyclase Catalysis: An ab Initio QM/MM MD Study, *J.Chem.Theory Comput. 10*, 1109-1120.
22. Zhang, Y. K. (2006) Pseudobond ab initio QM/MM approach and its Applications to Enzyme Reactions, *Theor. Chem. Acc. 116*, 43-50.

23. Zhang, Y. K., Lee, T. S., and Yang, W. T. (1999) A Pseudobond Approach to Combining Quantum Mechanical and Molecular Mechanical Methods, *J. Chem. Phys. 110*, 46-54.
24. Zhang, Y. K., Liu, H. Y., and Yang, W. T. (2000) Free energy calculations on enzyme reactions with an efficient iterative procedure to determine minimum energy paths on a combined ab initio QM/MM potential, *J. Chem. Phys. 112*, 3483-3492.
25. Zhang, Y. K. (2005) Improved pseudobonds for combined ab initio quantum mechanical/molecular mechanical methods, *J. Chem. Phys. 122*, 024114.
26. Beeman, D. (1976) Some multistep methods for use in molecular dynamics calculations, *J. Comput. Phys. 20*, 130-139.
27. Shao, Y., Molnar, L. F., Jung, Y., Kussmann, J. O. C., Brown, S. T., Gilbert, A. T., Slipchenko, L. V., Levchenko, S. V., O'Neill, D. P., DiStasio, R. A., Lochan, R. C., Wang, T., Beran, G. J., Besley, N. A., Herbert, J. M., Lin, C. Y., Van Voorhis, T., Chien, S. H., Sodt, A., Steele, R. P., Rassolov, V. A., Maslen, P. E., Korambath, P. P., Adamson, R. D., Austin, B., Baker, J., Byrd, E. F., Dachsel, H., Doerksen, R. J., Dreuw, A., Dunietz, B. D., Dutoi, A. D., Furlani, T. R., Gwaltney, S. R., Heyden, A., Hirata, S., Hsu, C. P., Kedziora, G., Khalliulin, R. Z., Klunzinger, P., Lee, A. M., Lee, M. S., Liang, W., Lotan, I., Nair, N., Peters, B., Proynov, E. I., Pieniazek, P. A., Rhee, Y. M., Ritchie, J., Rosta, E., Sherrill, C. D., Simmonett, A. C., Subotnik, J. E., Woodcock, H. L., Zhang, W., Bell, A. T., Chakraborty, A. K., Chipman, D. M., Keil, F. J., Warshel, A., Hehre, W. J., Schaefer, H. F., Kong, J., Krylov, A. I., Gill, P. M., and Head-Gordon, M. (2006) *Q-Chem,version 3.0,Q-chem,Inc.: Pittsburgh, PA*.
28. Ponder, J. W. (2004) *TINKER, Software Tools for Molecular Design,Version 4.2*.
29. Torrie, G. M., and Valleau, J. P. (1977) Nonphysical sampling distributions in Monte Carlo free-energy estimation: Umbrella sampling, *J. Comput. Phys. 23*, 187-199.
30. Vijayaraj, R., Van Damme, S., Bultinck, P., and Subramanian, V. (2012) Molecular dynamics and umbrella sampling study of stabilizing factors in cyclic peptide-based nanotubes, *J. Phys. Chem. B 116*, 9922-9933.
31. Souaille, M., and Roux, B. (2001) Extension to the weighted histogram analysis method: combining umbrella sampling with free energy calculations, *Comput. Phys. Commun. 135*, 40-57.
32. Kumar, S., Bouzida, D., Swendsen, R. H., Kollman, P. A., and Rosenberg, J. M. (1992) Liquid-liquid transition in ST2 water, *J. Comput. Chem. 13*, 1011-1021.

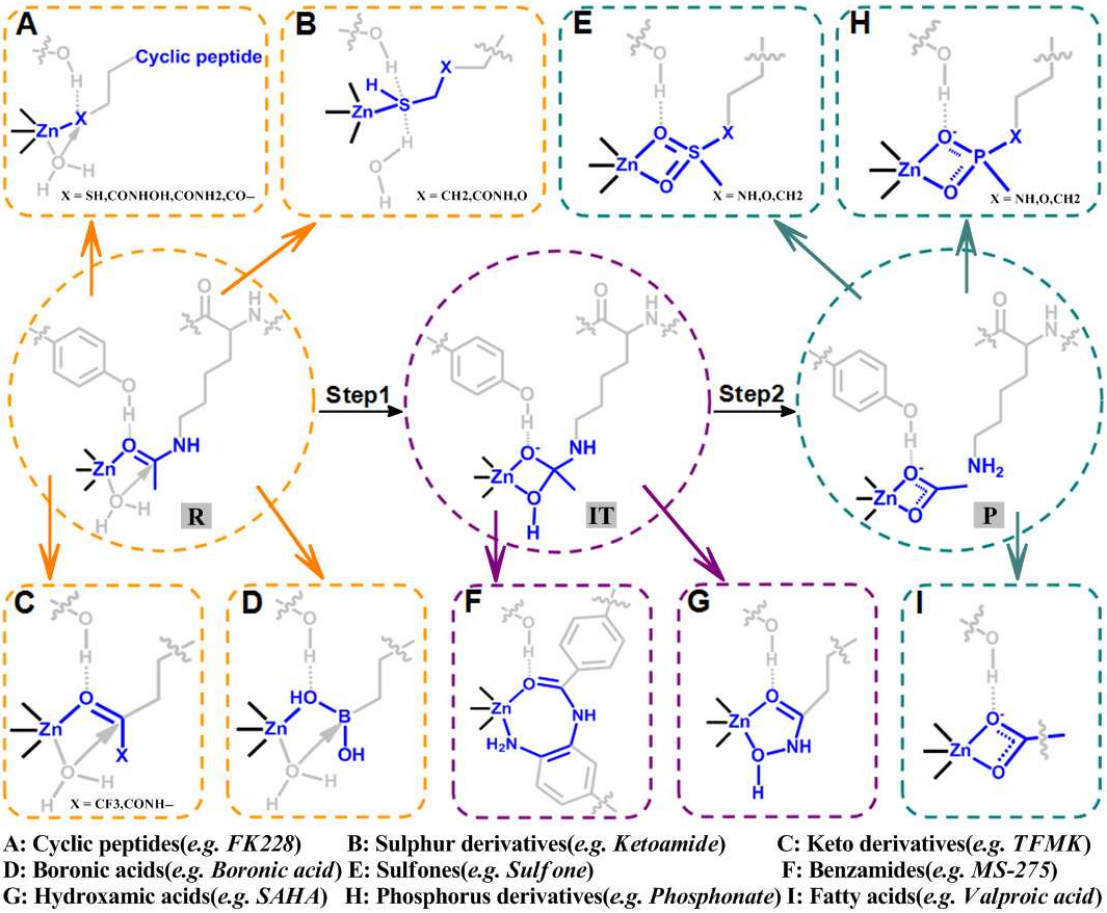

Figure S1. Chemical classification of HDAC inhibitors based on reactant (R), intermediate (IT) and product (P) state of the lysine deacetylation reaction. The lysine deacetylation reaction is exhibited in circles with different colors, and the HDAC inhibitors shown in rectangle with corresponding colors. The Zn ion and chelating area of HDAC inhibitors are highlighted in blue.

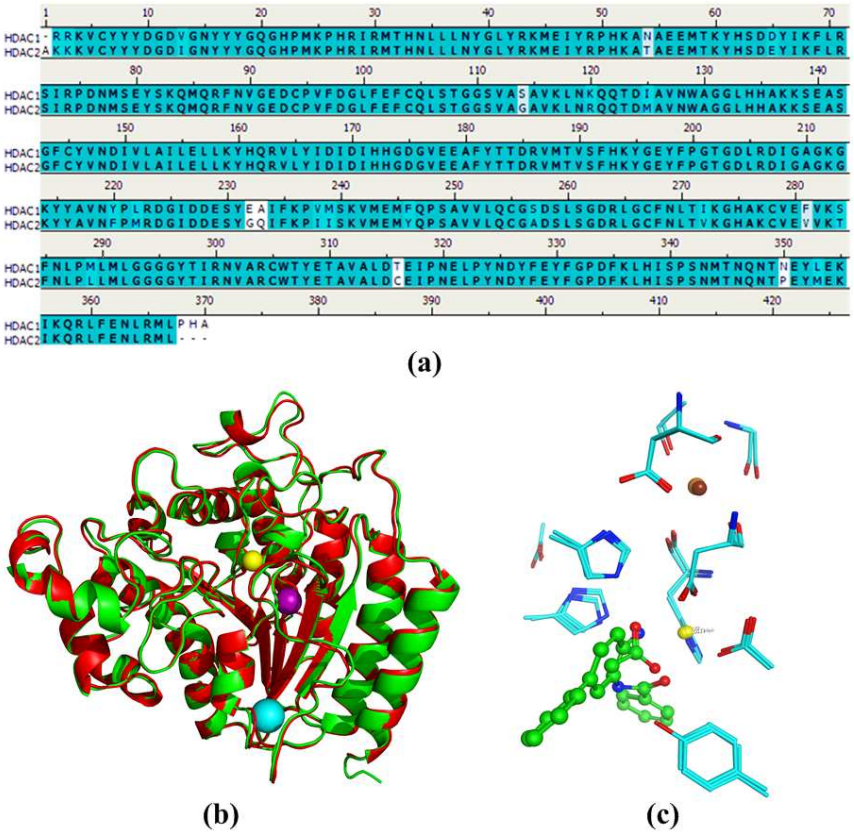

Figure S2. The sequence alignment (a) and structure alignment (b,c) of HDAC1 (pdb code: 4BKX) and HDAC2 (pdb code: 3MAX). The sequence identity is 93.5% and similarity is 97.8%, the RMSD of protein and active-site alignment for all heavy atoms is 0.7 Å and 0.6 Å respectively. (Analyzed by Discover Studio 3.5 package)

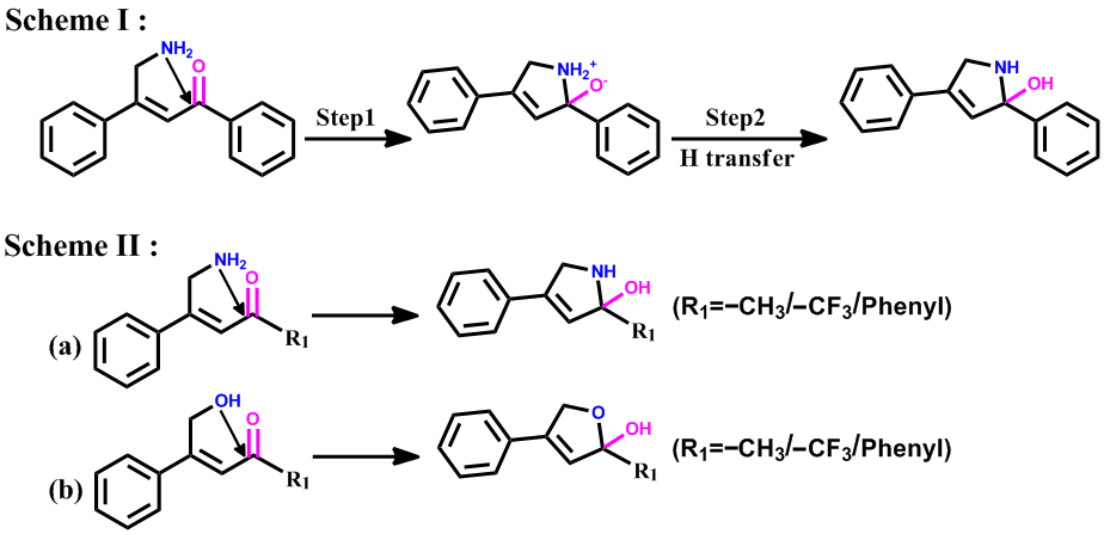

Figure S3. The possible reaction pathways for the intramolecular-nucleophilic-attack. Scheme I: stepwise mechanism; Scheme II: concerted mechanism.

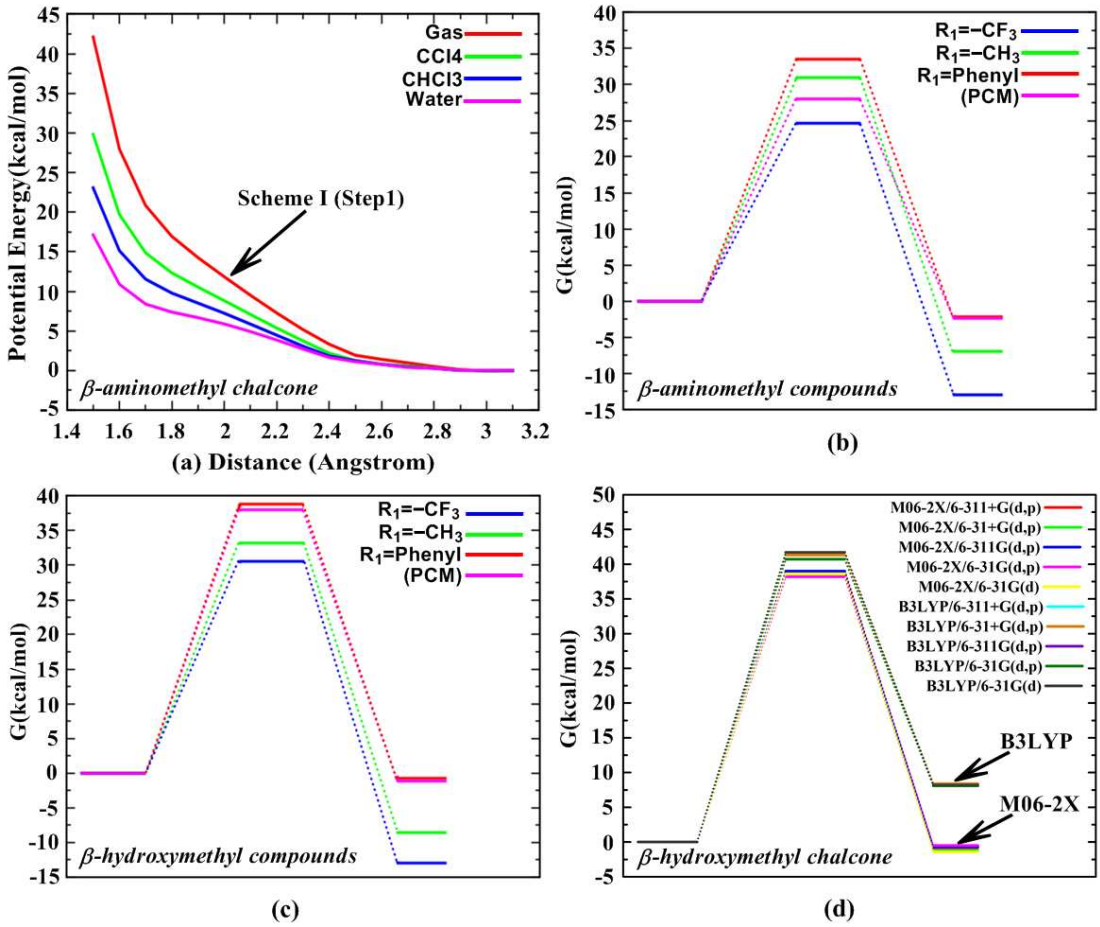

Figure S4. (a) The relative energy profiles of the stepwise mechanism. It indicates that stepwise mechanism is unreasonable. (b) The relative energy profiles of the concerted mechanisms for the *β*-aminomethyl compounds, namely scheme II (a) in Figure S3. (c) The relative energy profiles of the concerted mechanism for the β-hydroxymethyl compound, namely scheme II (b) in Figure S3. (d) The benchmark test on M06-2X vs B3LYP methods with various basis set for the *β*-hydroxymethyl compound. It indicates that B3LYP is prefer to underestimate the relative stability of the cyclic product, and it also indicates that the basis set dependence is very small for M06-2X methods. It is also confirmed in our further QM/MM calculations, as shown in Figure S7 (e-f).

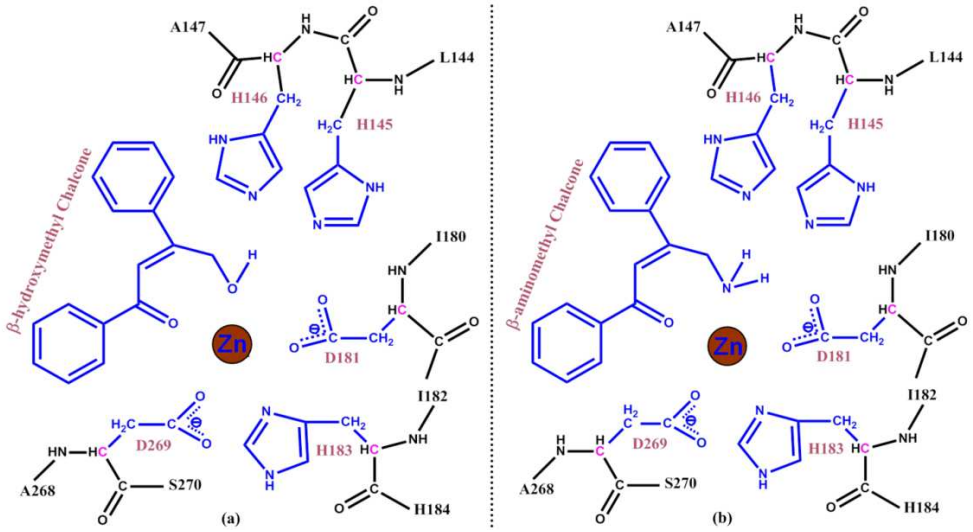

Figure S5. The detailed QM/MM partition schemes for *ab initio* QM/MM MD simulations. (black, MM subsystem; pink, boundary carbon atoms in QM subsystem described by improved pseudobond parameters; blue, all other atoms in the QM subsystem.)

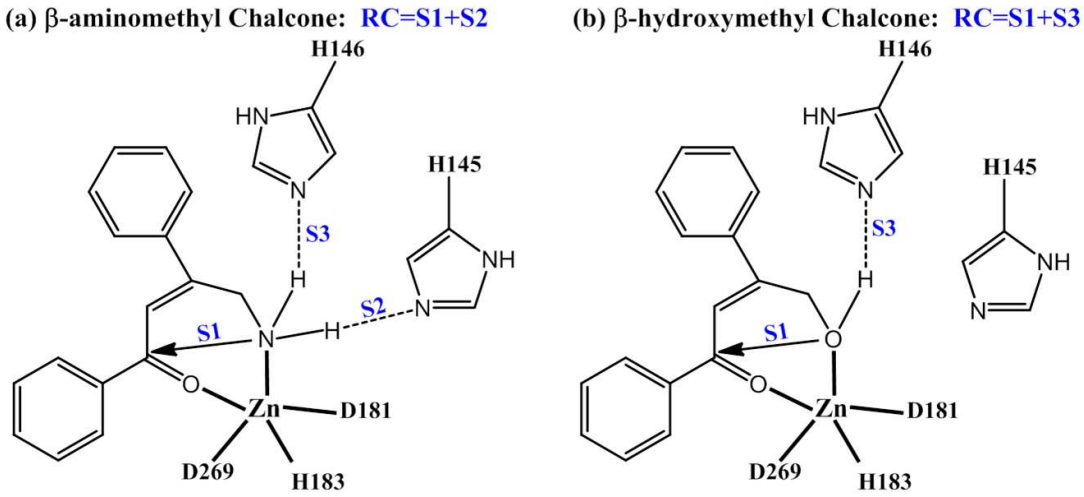

Figure S6. Illustration of the reaction coordinate (RC) chosen for the intramolecular nucleophilic attack reaction in the *ab initio* QM/MM studies. Both the RC=S1+S2 and RC=S1+S3 were tried for the *β*-aminomethyl chalcone and benzamide, then the RC=S1+S2 was finally employed for the *β*-aminomethyl chalcone and the relative systems (R_1=CH_3 and CF_3) by considering the potential energy profiles results (see Figure S7). For the *β*-hydroxymethyl chalcone, the RC=S1+S3 was employed since the single hydrogen bond with H146 is very stable during the QM/MM MD simulations.

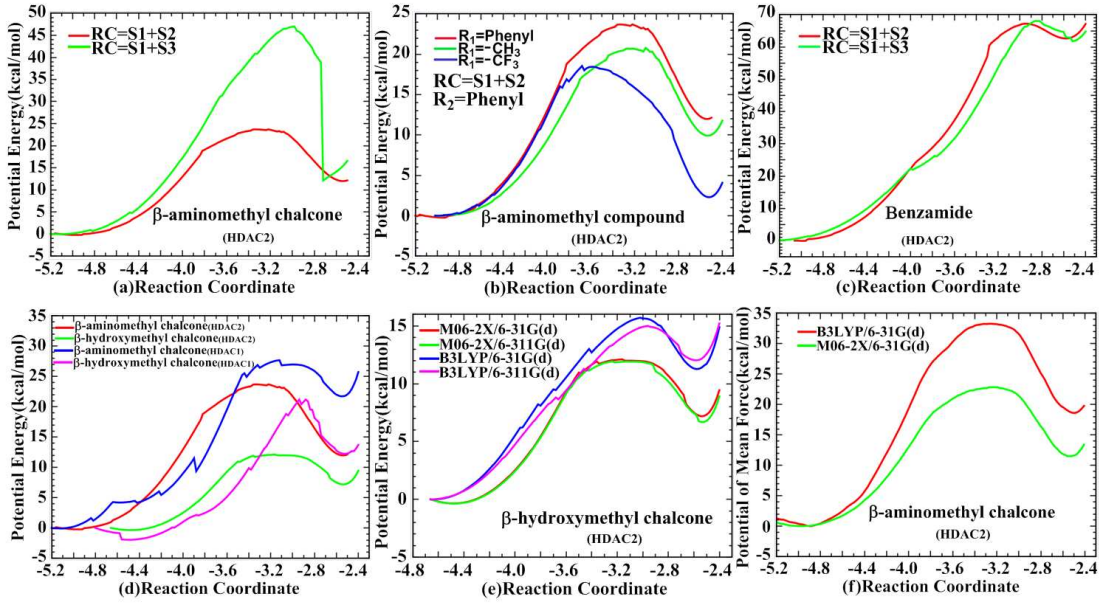

Figure S7. The minimum energy paths for the selected compounds under enzymatic catalysis (a-d), and the benchmark test on M06 and B3LYP methods for the selected enzymatic models (e-f, conclusion is similar to the gas phase results as shown in Figure S4(d)). Herein, R_1, R_2 refer to Figure 1 and RC refer to Figure S6.

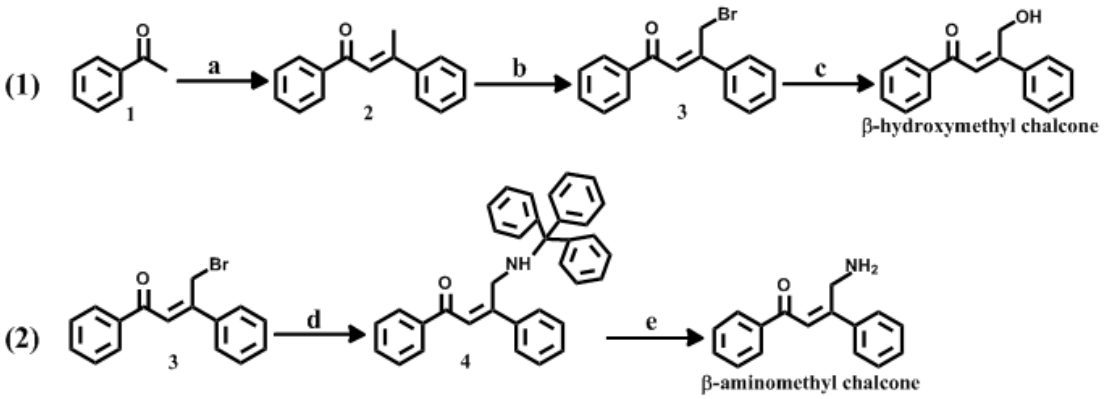

Figure S8. Synthesis of the *β*-substituted chalcones. Reagents and reaction conditions: (a) absolute EtOH, $SOCl_2$, rt, 2h; (b) NBS/BPO, CCl_4, heat, reflux, 5h; (c) CH_3COONa, absolute MeOH, heat, reflux, 24h; (d) Tritylamine, acetonitrile, triethylamine, N_2, heat, reflux, 24h; (e) 60% CH_2Cl_2/ CF_3COOH, rt, 24h.

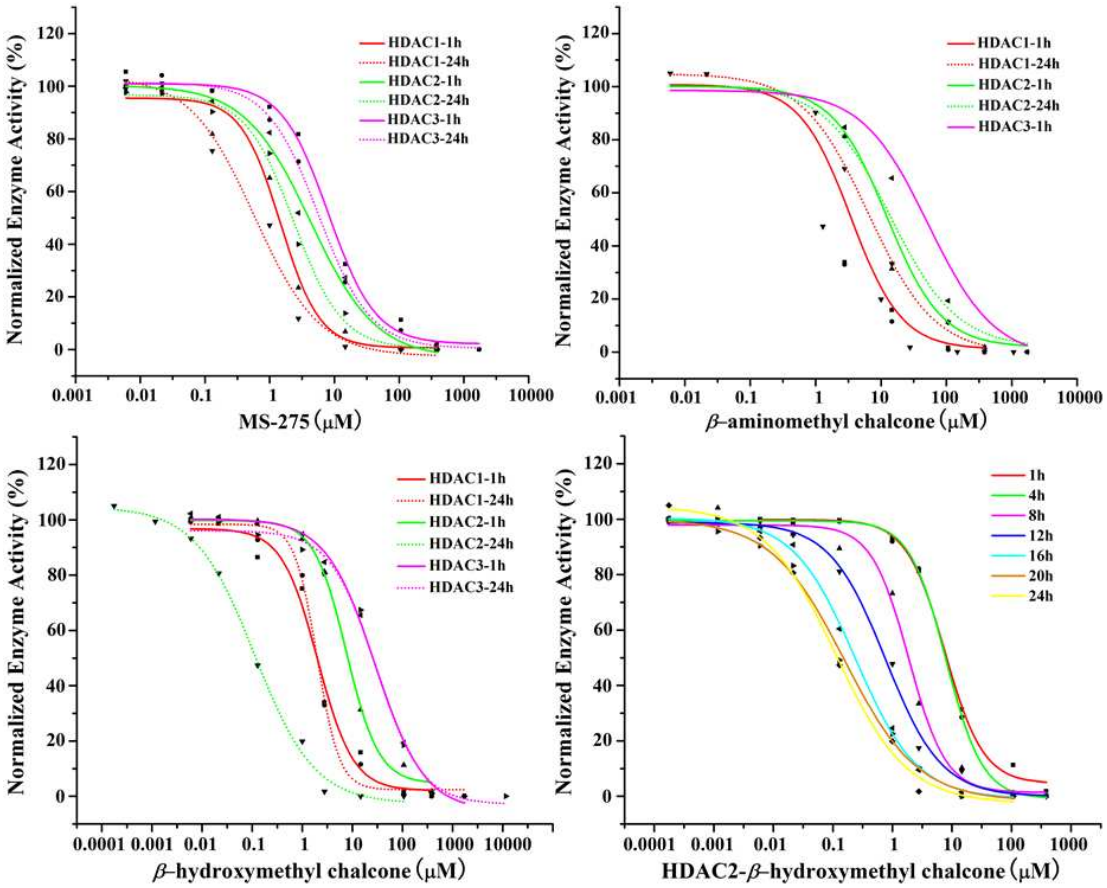

Figure S9. Dose-response curves of the designer β-substituted chalcones and positive control MS-275.

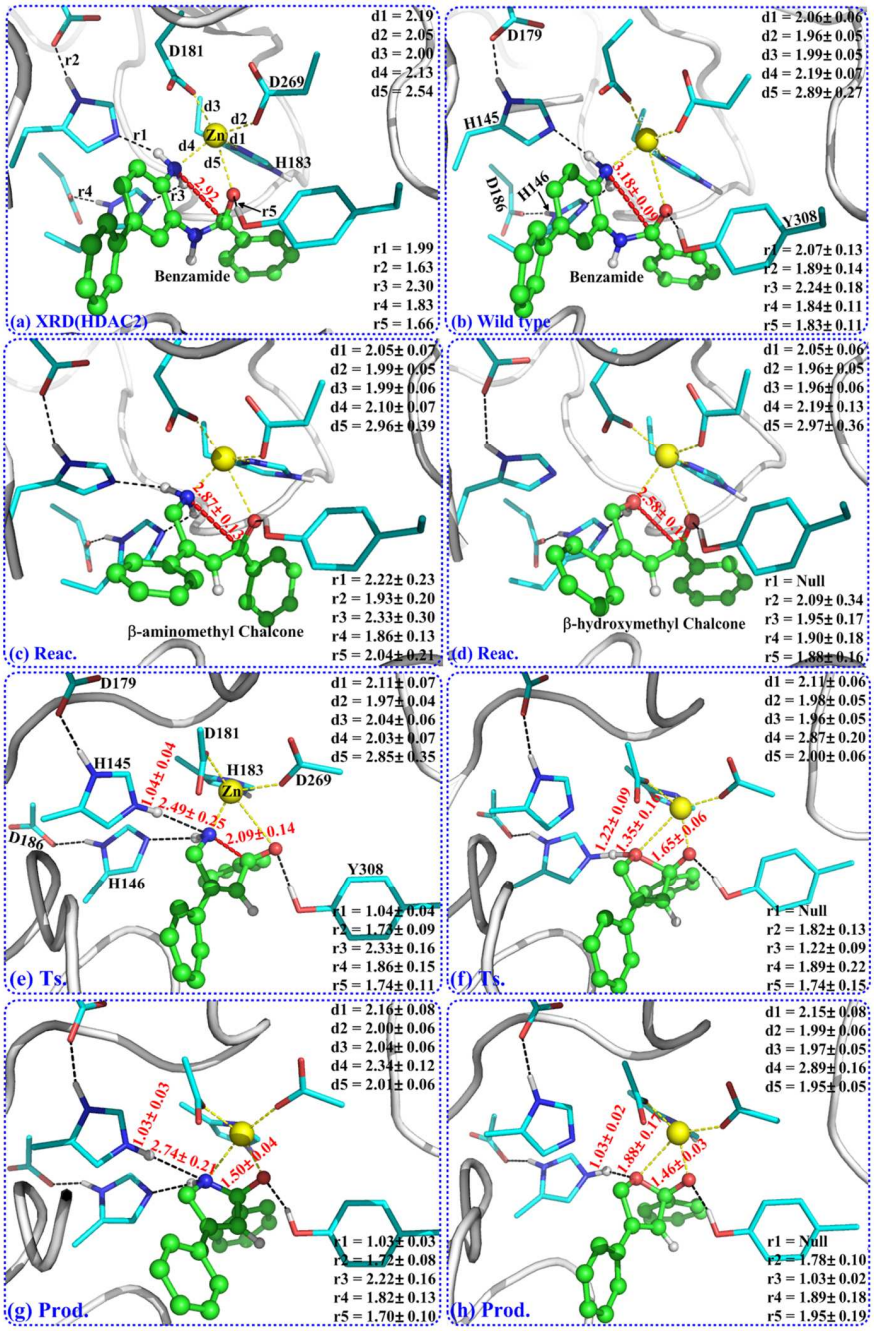

Figure S10. Illustration of the zinc chelation modes and hydrogen bond network. (a) is the HDAC2 XRD structure and (b) is the corresponding QM/MM MD results. The (c)(e)(g) present the reaction states for the *β*-aminomethyl chalcone-HDAC2 model and (d)(f)(h) present for the *β*-hydroxymethyl chalcone-HDAC2 model from QM/MM MD simulations. The distance between nucleophilic atoms (N1 and O1) and carbonyl carbon (C5) of ligands is highlighted in red.

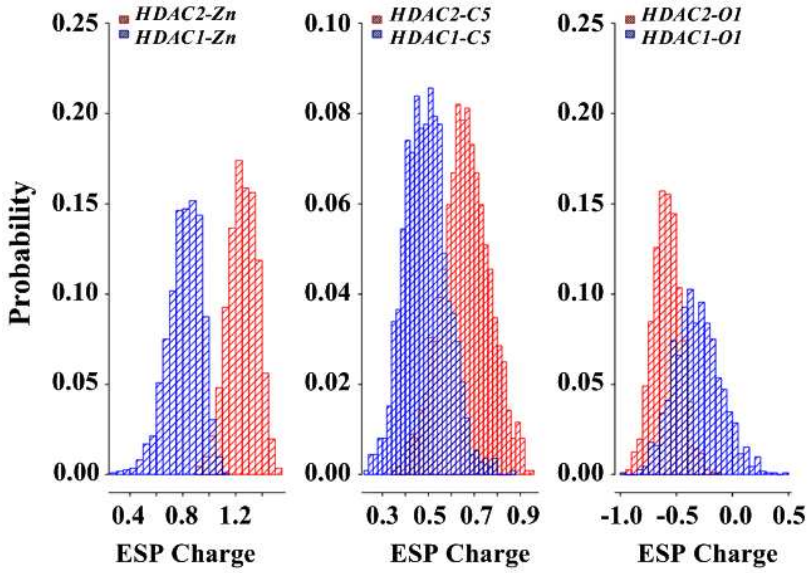

Figure S11. The ESP charge distribution of the selected atoms in the *β*-hydroxymethyl chalcone-HDAC1/2 complexes. (Zn, C5, O1 refer to Figure 2).

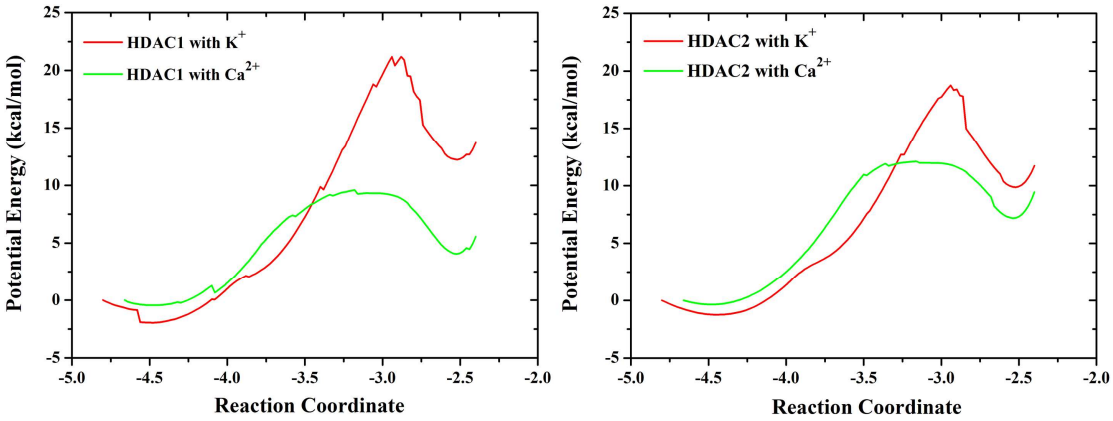

Figure S12. The minimum energy paths for the β-hydroxymethyl chalcone in HDAC1/2 with different metal ions.

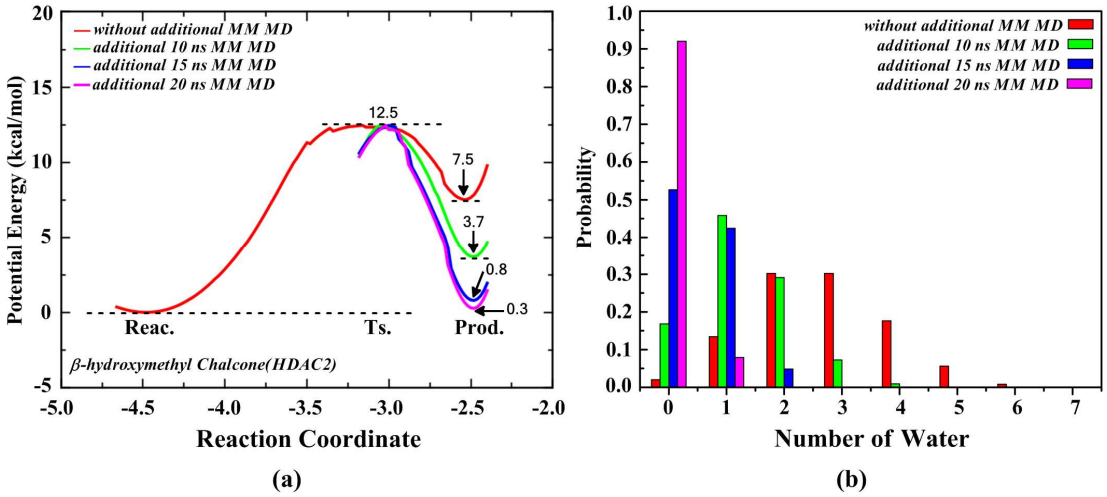

Figure S13. (a) The comparison of relative reaction profiles with additional classical MD simulations on the final product state in the *β*–hydroxymethy chalcone model. (b) The number of water molecules near the binding pocket at the final product state with additional classical MD simulations.

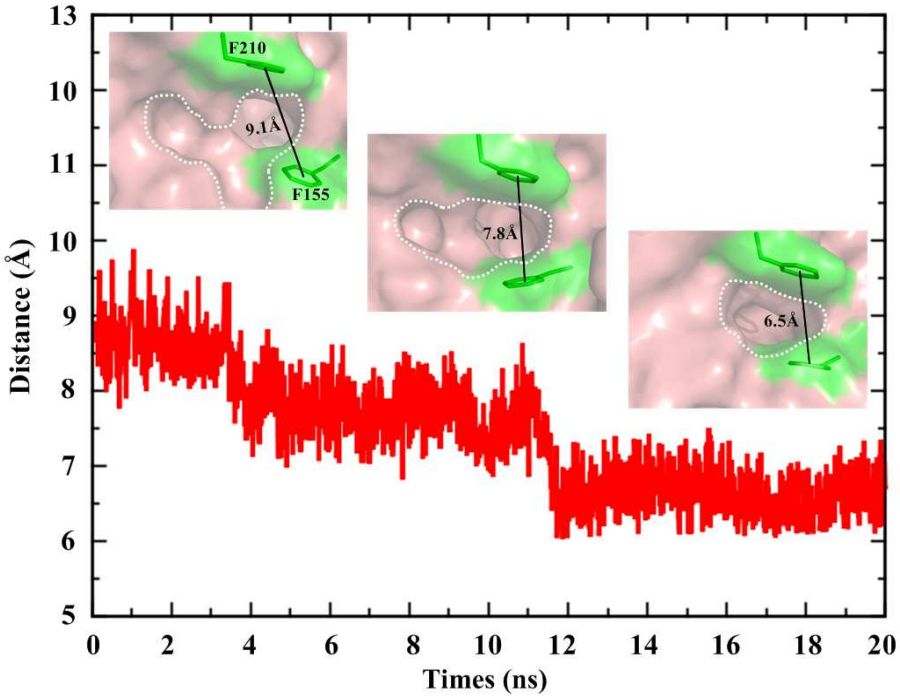

Figure S14. The representative π-π stacking and the pocket shape at the final product state along the 20 ns additional MM MD simulations.

Table S1. The intramolecular nucleophilic-attack reactivity of the designers (shown in Figure 2). All computational details refer to Figure S3-S7.

Simulation Model	Reactivity (relative reaction barrier, unit: kcal/mol)						
	β-aminomethyl compound			*β*-hydroxymethyl compound			Benzamide
	R1=-CF3 R2=Phenyl	R1=-CH3 R2=Phenyl	R1=R2=Phenyl (chalcone)	R1=-CF3 R2=Phenyl	R1=-CH3 R2=Phenyl	R1=R2=Phenyl (chalcone)	R1=Phenyl R2=Biphenyl
Gas-phase	medium (24.6)	low (31.0)	low (33.5)	low (30.6)	low (33.2)	no (38.8)	-
Solvent	-	-	low (28.0)	-	-	no (38.0)	-
HDAC2	high (17.2)	medium (21.1)	medium (23.7)	-	-	very high (12.1)	no (68.1)
HDAC1	-	-	low (27.7)	-	-	medium (21.2)	-